Proceedings of 9th International Symposium on Fluid-Structure Interactions, Flow-Sound Interactions, Flow-Induced Vibration & Noise
July 8-11, 2018, Toronto, Ontario, Canada

FIV2018-138

NONLINEAR DYNAMICS OF A HANGING CANTILEVERED PIPE SIMULTANEOUSLY SUBJECTED TO INTERNAL AND EXTERNAL AXIAL FLOWS

Ahmed R. Abdelbaki
Mechanical Engineering Department
McGill University
Montreal, QC, H3A 2K6
Canada
ahmed.abdelbaki@mail.mcgill.ca

Arun K. Misra
Mechanical Engineering Department
McGill University
Montreal, QC, H3A 2K6
Canada
arun.misra@mcgill.ca

Michael P. Païdoussis
Mechanical Engineering Department
McGill University
Montreal, QC, H3A 2K6
Canada
michael.paidoussis@mcgill.ca

ABSTRACT

A nonlinear model for the dynamics of a hanging cantilevered pipe simultaneously subjected to internal and external axial flows is developed in this paper. The pipe discharges fluid downwards, which then flows upwards through an annular region contained by a rigid channel. Thus, the external flow is dependent on the internal one, and confined over the whole length of the cantilever. A nonlinear equation of motion is derived for that system via Hamilton's principle to third-order accuracy. The fluid-related forces associated with the external flow are derived separately, as well as the non-conservative forces due to the internal flow. The equation of motion is discretized utilizing Galerkin's technique and solved numerically. The solution is presented by means of bifurcation diagrams, time histories, power-spectral-densities and phase-plane plots. The results are compared to those presented in experimental and linear theoretical studies from the literature having the same system parameters. It was found that the nonlinear theory can qualitatively predict the same dynamical behaviour as observed, and is in reasonable quantitative agreement with the recorded data. Moreover, this model provides a better estimation of the onset of instability compared to the linear one.

NOMENCLATURE

A_{ch}	Cross-sectional area of the annular region
A_i, A_o	Inner and outer cross-sectional areas of the pipe
C_{Dp}	Form-drag coefficient
C_N, C_T	Normal and tangential drag coefficients
D_{ch}	Inner diameter of the rigid channel
D_h	Hydraulic diameter of the cantilever
D_i, D_o	Inner and outer diameter of the hanging pipe
EI	Flexural rigidity of the hanging pipe
k	Viscous damping coefficient
L	Length of the hanging pipe
m	Mass of the pipe per unit length
M_i	Mass of the internal fluid per unit pipe length
M_o	Virtual added mass per unit pipe length related to the external flow
p_i, p_o	Internal and external fluid pressures
ρ	Fluid density
$T_o(L)$	Applied tension at the free end of the pipe
U_i, U_o	Internal and external flow velocities

INTRODUCTION

Pipes simultaneously subjected to internal and external axial flows can be found in many industrial appli-

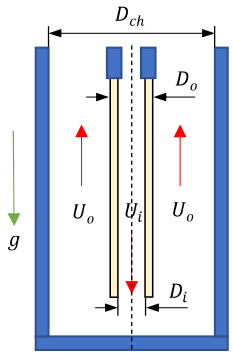

FIGURE 1: DIAGRAMMATIC OF THE HANGING CANTILEVERED PIPE UNDER STUDY.

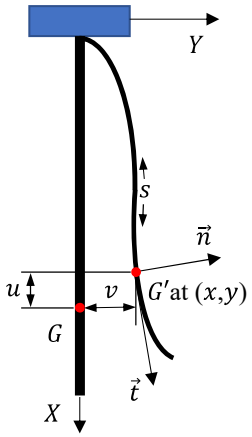

FIGURE 2: DIAGRAM DEFINING THE COORDINATE SYSTEMS USED.

cations, e.g., heat exchangers and drill stings. The first study on that topic was undertaken by Cesari and Curioni [1]. In that short article, the stability of horizontal tubes with different boundary conditions was investigated theoretically. Païdoussis et al. [2] examined the linear dynamics of a long tubular cantilever that discharges fluid downwards which then flows upwards as a confined external flow. Rinaldi [3] studied the same configuration experimentally and derived a linear model for its dynamics; however, a large discrepancy was found between the theory and the experiments regarding the critical flow velocity of instability. Recently, Fujita and Moriasa [4] employed the principle of superposition of the linear stability analysis of a pipe subjected to internal and external flows separately to examine the dynamics of the same system.

In this paper, the dynamics of a hanging cantilevered pipe simultaneously subjected to counter-current, interdependent internal and confined external axial flows, as shown in Fig. 1, is examined using a nonlinear theory for the first time. The equation of motion is derived in the following sections, and it is solved for a system having the same parameters as that experimentally tested in [3].

DERIVATION OF THE THEORETICAL MODEL

The system under study consists of a flexible cantilevered pipe that is centrally located in a cylindrical rigid channel, so that its undeformed axis coincides with the gravity direction, g, as shown in Fig. 1. The pipe is assumed to be slender and can be modeled using Euler-Bernoulli beam theory. Also, the flow is assumed to be uniform and the external flow velocity is related to the internal one via the continuity equation. In addition, the motion of the pipe is assumed to be planar with large deflections, but small strains.

In the following analysis, two coordinate systems are used: (i) the Lagrangian (X, Y, Z, t), which is associated with the undeformed state of the cantilever, and (ii) the Eulerian (x, y, z, t) for the deformed state. The displacements of a material point on the centreline of the cantilever, G, from the undeformed state to the deformed one are shown in Fig. 2, where $u = x - X$, $v = y - Y$, and $w = z - Z$. The pipe centreline motions are assumed to be in the (X-Y)-plane, hence $Y = 0$ and $z = Z = w = 0$. The curvilinear coordinate along the cantilever, s, can be related to X by $\frac{\partial s}{\partial X} = 1 + \tilde{\varepsilon}$, where $\tilde{\varepsilon}$ is the axial strain along the centreline with $1 + \tilde{\varepsilon}(X) = [(\frac{\partial x}{\partial X})^2 + (\frac{\partial y}{\partial X})^2]^{1/2}$. Since, the pipe centreline is assumed to be inextensible, then $\tilde{\varepsilon} = 0$, $\frac{\partial s}{\partial X} = 1$ and $(\frac{\partial x}{\partial X})^2 + (\frac{\partial y}{\partial X})^2 = 1$.

The equation of motion is derived via Hamilton's principle,

$$\delta \int_{t_1}^{t_2} \mathscr{L}\, \mathrm{d}t + \int_{t_1}^{t_2} \delta W\, \mathrm{d}t = 0, \tag{1}$$

where $\mathscr{L} = \mathscr{T}_p - \mathscr{V}_p$ is the Lagrangian, $\mathscr{T}_p$ is the kinetic energy of the pipe including the conveyed fluid, $\mathscr{V}_p$ is its potential energy, $\delta W = \delta W_i + \delta W_o$ is the total virtual work done on the pipe, δW_i is the virtual work due to the non-conservative forces associated with the internal flow, which are not included in the Lagrangian, and δW_o is the virtual work due to the fluid-related forces associated with the external flow. The equation of motion obtained in this study is correct to third-order of magnitude, $\mathscr{O}(\varepsilon^3)$, for $y = v \sim \mathscr{O}(\varepsilon)$ and $u \sim \mathscr{O}(\varepsilon^2)$. Hence the expressions for

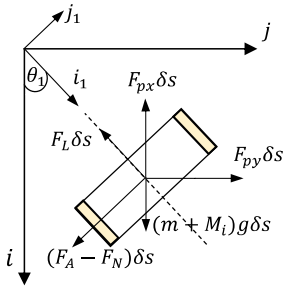

FIGURE 3: FORCES ACTING ON A PIPE ELEMENT.

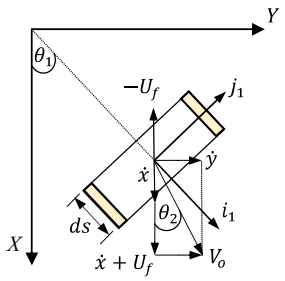

FIGURE 4: RELATIVE FLUID-BODY VELOCITY V_o.

the virtual work must be correct to $\mathscr{O}(\varepsilon^3)$, while the energy expressions to $\mathscr{O}(\varepsilon^4)$.

Nonlinear expressions for the kinetic and potential energies of a pipe conveying fluid have been derived before in [5], as well as for the virtual work due to the non-conservative forces associated with the discharged flow. The fluid-related forces associated with external flow are derived separately in a similar manner as in [6]. An element of the deformed pipe is subjected to the following forces, as shown in Fig. 3: the inviscid fluid dynamic force $F_A\delta s$, the normal and longitudinal viscous forces, $F_N\delta s$ and $F_L\delta s$, respectively, and the hydrostatic forces in the x- and y-direction, $F_{px}\delta s$ and $F_{py}\delta s$, respectively.

The inviscid hydrodynamic forces are derived using an extension of Lighthill's linear slender-body potential flow theory formulated in [7] to a third-order nonlinear formulation, taking into account the inverted direction of the external flow in the problem at hand. Thus,

$$\begin{aligned} F_A(X,t) = &\left\{\frac{\partial}{\partial t}+\left[-U_o(1-\frac{\partial u}{\partial X})-(\frac{\partial u}{\partial t}-U_o)\frac{\partial u}{\partial X}\right]\frac{\partial}{\partial X}\right\} \\ &\times\left[V_o-(\frac{\partial u}{\partial t}\frac{\partial v}{\partial X}-2U_o\frac{\partial u}{\partial X}\frac{\partial v}{\partial X}) \right. \\ &\left.-\frac{1}{2}V_o(\frac{\partial v}{\partial X})^2\right]M_o-\frac{1}{2}M_oV_o\frac{\partial v}{\partial X}\frac{\partial V_o}{\partial X}+\mathscr{O}(\varepsilon^5), \end{aligned} \tag{2}$$

where V_o is the relative fluid-body velocity associated with the external flow and M_o is the virtual added mass, which is equal to $\chi\rho A_o$, while $\chi=(D_{ch}^2+D_o^2)/(D_{ch}^2-D_o^2)$ is the confinement parameter. Defining the unit vector pair $(\vec{i}_1,\ \vec{j}_1)$, which is in the tangential and normal to the centreline directions at angle θ_1 to $(\vec{i},\ \vec{j})$, as shown in Fig. 3, θ_1 can be written as $\theta_1=y'-u'y'-\frac{1}{3}y'^3+\mathscr{O}(\varepsilon^5)$ with $(\ )'=\frac{\partial(\ )}{\partial s}$. The velocity of the cantilever with respect to the velocity of the fluid can be defined as $\vec{V}_o=\vec{y}+\vec{x}-(-\vec{U}_f)$, and its direction is shown in Fig. 4, where $U_f=U_o(1-\frac{\partial u}{\partial X})$ is the mean axial flow velocity relative to the deforming cantilever. Hence, we have

$$V_o=\dot{y}-U_oy'-\frac{1}{2}\dot{y}y'^2+2U_ou'y'+\frac{1}{2}U_oy'^3-\dot{x}y'+\mathscr{O}(\varepsilon^5), \tag{3}$$

where $(\ )'=\frac{\partial(\ )}{\partial s}$ and $(\dot{\ })=\frac{\partial(\ )}{\partial t}$.

The viscous forces are obtained on the basis of the semi-empirical expressions proposed by Taylor [8]. Following the procedure described in [6], one can write

$$\begin{aligned} F_N=&\frac{1}{2}\rho D_oU_o^2\left[C_N\left(y'-\frac{\dot{y}}{U_o}-\frac{\dot{y}u'}{U_o}-u'y'+\frac{\dot{x}\dot{y}}{U_o^2}\right.\right. \\ &\left.-\frac{1}{2}\left(y'^3-\frac{\dot{y}^3}{U_o^3}-\frac{y'^2\dot{y}}{U_o}+\frac{y'\dot{y}^2}{U_o^2}\right)\right) \\ &\left.-C_{Dp}\left(y'|y'|+\frac{y'|\dot{y}|+|y'|\dot{y}}{U_o}+\frac{\dot{y}|\dot{y}|}{U_o^2}\right)\right]+k\dot{y}+\mathscr{O}(\varepsilon^5), \\ F_L=&\frac{1}{2}\rho D_oU_o^2C_T\left[1-\frac{1}{2}\left(y'^2-2\frac{y'\dot{y}}{U_o}+\frac{\dot{y}^2}{U_o^2}\right)\right]+\mathscr{O}(\varepsilon^4). \end{aligned} \tag{4}$$

In addition, a detailed derivation of the hydrostatic forces is also provided in [6] for a clamped-free cylinder in axial flow, which can be utilized to obtain the following expressions for the case here under study:

$$\begin{aligned} -F_{px}=&y'^2\left(-\frac{1}{2}\rho D_oU_o^2C_T\frac{D_o}{D_h}-\rho gA_o\right)-y'y''A_op_o \\ &+\mathscr{O}(\varepsilon^4), \\ F_{py}=&(y'-u'y'-y'^3)\left(\frac{1}{2}\rho D_oU_o^2C_T\frac{D_o}{D_h}+\rho gA_o\right) \\ &+(y''-u''y'-u'y''-\frac{3}{2}y'^2y'')A_op_o+\mathscr{O}(\varepsilon^5). \end{aligned} \tag{5}$$

The virtual work due to the fluid-related forces associated with the external flow can be written as

$$\int_{t_1}^{t_2}\delta W_o \mathrm{d}t = \int_{t_1}^{t_2}\int_0^L \{[-F_{px}-F_L\cos\theta_1 + (F_A-F_N)\sin\theta_1]\delta x + [F_{py}-F_L\sin\theta_1 - (F_A-F_N)\cos\theta_1]\delta y\}\,\mathrm{d}s\,\mathrm{d}t. \tag{6}$$

By substituting Eqs. 2-5 into Eq. 6, and using Eq. 1, the final equation of motion of the system can be derived after many manipulations and transformations. Defining the following dimensionless quantities:

$$\xi=\frac{s}{L},\quad \eta=\frac{y}{L},\quad \tau=\left(\frac{EI}{m+M_i+\rho A_o}\right)^{1/2}\frac{t}{L^2},$$
$$u_i=\left(\frac{M_i}{EI}\right)^{1/2}U_iL,\quad u_o=\left(\frac{\rho A_o}{EI}\right)^{1/2}U_oL,$$
$$\beta_i=\frac{M_i}{m+M_i+\rho A_o},\quad \beta_o=\frac{\rho A_o}{m+M_i+\rho A_o},$$
$$\gamma=\frac{(m+M_i-\rho A_o)gL^3}{EI},\quad \Gamma=\frac{T_o(L)L^2}{EI},\quad c_N=\frac{4}{\pi}C_N,$$
$$c_T=\frac{4}{\pi}C_T,\quad c_d=\frac{4}{\pi}C_{Dp},\quad \bar{\varepsilon}=\frac{L}{D_o},\quad h=\frac{D_o}{D_h},$$
$$\alpha=\frac{D_i}{D_o},\quad \alpha_{ch}=\frac{D_{ch}}{D_o},\quad \Pi_{iL}=\frac{A_ip_i(L)L^2}{EI},$$
$$\Pi_{oL}=\frac{A_op_o(L)L^2}{EI},\quad \kappa=\frac{kL^2}{EI(m+M_i+\rho A_o)^{1/2}}, \tag{7}$$

the equation of motion can be written in dimensionless form, as follows:

$$\begin{aligned}
&[1+(\chi-1)\beta_o]\ddot{\eta}+2u_i\sqrt{\beta_i}\dot{\eta}'(1+\eta'^2)\\
&-2u_o\sqrt{\beta_o}\chi\dot{\eta}'(1-\frac{1}{4}\eta'^2)+u_o^2\chi\eta''(1+2\eta'^2)\\
&+u_i^2\eta''(1+\eta'^2)-\frac{3}{2}\chi\dot{\eta}\eta'(\beta_o\dot{\eta}'-u_o\sqrt{\beta_o}\eta'')\\
&-\frac{1}{2}u_o^2\bar{\varepsilon}c_N[\eta'+\frac{1}{2}\eta'^3]+\frac{1}{2}u_o^2\bar{\varepsilon}c_T(1-\xi)(\eta''+\frac{3}{2}\eta'^2\eta'')\\
&-\Pi_{oL}(\eta''+\eta'^2\eta'')-(\Gamma-\Pi_{iL})(\eta''+\frac{3}{2}\eta'^2\eta'')\\
&-(\frac{1}{2}u_o^2\bar{\varepsilon}c_Th-\gamma)[\eta'+\frac{1}{2}\eta'^3-(1-\xi)(\eta''+\frac{3}{2}\eta'^2\eta'')]\\
&+\eta''''+4\eta'\eta''\eta'''+\eta''^3+\eta''''\eta'^2\\
&+\frac{1}{2}\bar{\varepsilon}c_N\beta_o\dot{\eta}\int_0^\xi\eta'\dot{\eta}'\mathrm{d}s+\frac{1}{2}u_o^2\bar{\varepsilon}c_N\Big(\frac{\sqrt{\beta_o}}{u_o}\dot{\eta}+\frac{1}{2}\frac{\beta_o}{u_o^2}\dot{\eta}^2\eta'\\
&-\frac{1}{2}\frac{\sqrt{\beta_o}}{u_o}\dot{\eta}\eta'^2-\frac{1}{2}\frac{\beta_o^{3/2}}{u_o^3}\dot{\eta}^3\Big)+\kappa\dot{y}\\
&+\frac{1}{2}u_o^2\bar{\varepsilon}c_d\Big(\eta'|\eta'|+\frac{\sqrt{\beta_o}}{u_o}(\eta'|\dot{\eta}|+|\eta'|\dot{\eta})+\frac{\beta_o}{u_o}\dot{\eta}|\dot{\eta}|\Big)\\
&-\eta''(1-\beta_o)\int_\xi^1\int_0^\xi(\dot{\eta}'^2+\eta'\ddot{\eta}')\,\mathrm{d}\xi\,\mathrm{d}\xi\\
&+2\chi(\beta_o\dot{\eta}'-u_o\sqrt{\beta_o}\eta'')\int_0^\xi\eta'\dot{\eta}'\,\mathrm{d}\xi\\
&-\chi\eta''\int_\xi^1(\beta_o\ddot{\eta}\eta'-2u_o\sqrt{\beta_o}\dot{\eta}'\eta'+u_o^2\eta''\eta')\,\mathrm{d}\xi\\
&+\eta'(1+(\chi-1)\beta_o)\int_0^\xi(\dot{\eta}'^2+\eta'\ddot{\eta}')\,\mathrm{d}\xi\\
&+\eta''\int_\xi^1\{\Pi_{oL}\eta'\eta''-\frac{1}{4}\bar{\varepsilon}c_T\beta_o\dot{\eta}^2\}\,\mathrm{d}\xi\\
&-3\chi\sqrt{\beta_o}u_o\eta'\int_0^\xi(\eta'\dot{\eta}''+\eta''\dot{\eta}')\,\mathrm{d}\xi\\
&-\frac{1}{2}u_o^2\eta''(\bar{\varepsilon}c_T-\bar{\varepsilon}c_N)\int_\xi^1(\eta'^2-\frac{\sqrt{\beta_o}}{u_o}\eta'\eta_o)\,\mathrm{d}\xi\\
&-\eta''\int_\xi^1(2u_i\sqrt{\beta_i}\eta'\dot{\eta}'+u_i^2\eta'\eta'')\,\mathrm{d}\xi=0,
\end{aligned} \tag{8}$$

in which $(\,)'=\partial(\,)/\partial\xi$ and $\dot{(\,)}=\partial(\,)/\partial\tau$. It should be noted that the internal flow is related to the external one through continuity, thus we have $u_o=\alpha u_i/(\alpha_{ch}^2-1)$ and $\Pi_{iL}=\alpha^2\Pi_{oL}+\alpha u_o(\alpha u_o-u_i)$.

METHODS OF ANALYSIS

The equation of motion is discretized using Galerkin's technique, with the cantilever beam eigenfunctions, $\phi_j(\xi)$, as comparison functions and with $q_j(\tau)$ as the corresponding generalized coordinate; thus,

$$\eta(\xi,\tau)=\sum_{j=1}^{N}\phi_j(\xi)q_j(\tau), \tag{9}$$

where N represents the number of modes of Galerkin scheme. Substituting Eq. 9 into Eq. 8, multiplying by $\phi_i(\xi)$, and integrating over the domain $[0:1]$ results in a set of ordinary differential equations (ODEs). These ODEs are solved using AUTO [9], which is based on a

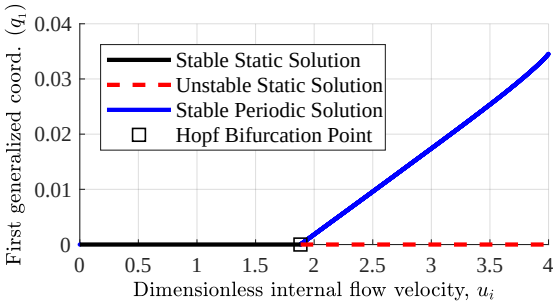

FIGURE 5: BIFURCATION DIAGRAM.

collocation method and is adapted to conduct bifurcation analysis for differential equations.

RESULTS AND DISCUSSION

In order to allow comparison between the results of the nonlinear model derived in this paper and the results of the experimental and theoretical study of Rinaldi [3], Eq. 8 is solved using system parameters similar to the ones in [3]. A system with the following parameters is considered: $D_o = 0.0159\,\text{m}$, $D_i = 0.00635\,\text{m}$, $L = 0.343\,\text{m}$, $EI = 1.05 \times 10^{-2}\,\text{N.m}^2$, $m = 0.355\,\text{kg/m}$, $M_i = 0.0317\,\text{kg/m}$, $\rho A_o = 0.198\,\text{kg/m}$, $\beta_o = 0.339$, $\beta_i = 0.0542$, $\alpha_{ch} = 1.6$, and $\gamma = 7.14$. In addition, $c_N = c_T = 0.0125$, $c_d = 1.25$, and $\kappa_j = \{4.2, 12.8, 20.3, 27.9\}$, which depends on the frequency of oscillations, as discussed in [2], thus a different value of κ is given for each mode, $j = 1:N$. The frequency of oscillations was estimated by conducting a linear analysis, finding the real part of the eigenfrequencies, and then calculating an average value for it at a specific range of flow velocities.

Figure 5 shows a bifurcation diagram obtained via a four-mode Galerkin approximation with q_1 being representative of the behaviour of the system. The pipe remains stable around the origin with increasing u_i, but at $u_i = 1.88$, a Hopf bifurcation is predicted leading to flutter in the first mode. The amplitude of oscillations increases almost linearly with increasing u_i. Samples of the time history and phase-plane plot at $u_i = 2.5$ are shown in Figs. 6 (a) and (b) revealing that the stable periodic oscillations are around the origin. Also, a power spectral density plot at the same flow velocity, calculated by direct fast Fourier transform, is shown in Fig. 6 (c) with one dominant frequency of oscillations. Moreover, the shape of the pipe at the maximum deflected position is plotted in Fig. 6 (d) showing that the oscillations are in the first mode.

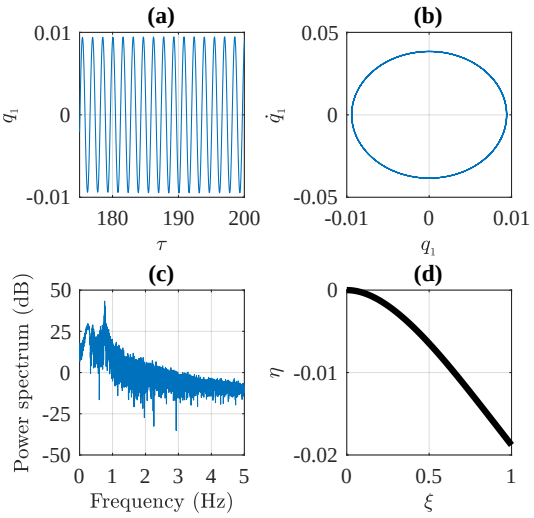

FIGURE 6: AT $u_i = 2.5$: (a) TIME HISTORY PLOT, (b) PHASE-PLANE PLOT, (c) POWER SPECTRAL DENSITY PLOT, and (d) SHAPE OF THE PIPE AT THE MAXIMUM DEFLECTED POSITION.

TABLE 1: Comparison between the values of the critical flow velocity for flutter, u_{if}, obtained by different studies.

	Experiments [3]	Theory [3]	Proposed Theory
u_{if}	0.21	2.3	1.88

The results obtained in this study are in good qualitative agreement with the experiments reported in [3], in which first-mode flutter was observed; and the amplitude of the oscillations increases linearly as the internal flow velocity is increased. However, quantitatively, flutter was observed experimentally at vanishing flow velocities as shown in Table 1. The linear analytical model derived in [3] predicts the same kind of instability, but overestimates its onset, at u_{if}, compared to the experiments and to this nonlinear theory, as shown in Table 1.

The linear model presented in [3] also predicts very weak damping at low flow velocities before flutter occurs, which can lead to flow-perturbation excitation at these low velocities. This could also be the case for the experimentally observed oscillations with small amplitudes at vanishing flow velocities. With increasing flow velocity, a sudden reduction in the recorded amplitude of oscillations in [3] is noticed at $u_i \approx 1.8$, which may indicate a

TABLE 2: Comparison between the maximum amplitude of flutter measured 160 mm below the clamped end of the pipe, $y_f(s = 0.466)$, in mm obtained by different studies.

u_i	y_f (Experiments [3])	y_f (Proposed Theory)
1.9	1.8212	0.0341
2.25	2.2009	1.1877
2.5	2.4620	1.9701

TABLE 3: Comparison between the frequency of oscillations, f, in Hz obtained by different studies.

u_i	f (Experiments [3])	f (Proposed Theory)
1.9	0.6978	0.1549
2.25	0.7073	0.7513
2.5	0.7172	0.7593

change to fluidelastic instability, namely flutter. This sudden reduction in the amplitude of the oscillations is also noticed in other experiments in [3] for the same system with different parameters.

The amplitude and the frequency of oscillations predicted by the proposed theory are also compared to the experimental data reported in [3] in Tables 2 and 3, receptively. The tables show a reasonable quantitative agreement between the theory and the experiments for the maximum amplitude of oscillations at flow velocities not too close to the onset of flutter, and also a good quantitative agreement for the frequency of oscillations.

CONCLUSION

A nonlinear analytical model for the dynamics of a hanging cantilevered pipe simultaneously subjected to internal and external axial flows has been derived for the first time. The model predicts, for a long flexible pipe in water flow, flutter in the first mode of the pipe at $u_{if} = 1.88$. The amplitude and the frequency of oscillations increase with increasing flow velocity. The results were compared to experimental data from the literature for a similar system with the same parameters; a good qualitative and reasonable quantitative agreement was found for the dynamical behaviour of the system.

ACKNOWLEDGEMENTS

The financial support by SMRI, PRCI and NSERC is gratefully acknowledged. The first author is also grateful to McGill University for a MEDA scholarship.

REFERENCES

[1] Cesari, F., and Curioni, S., 1971. "Buckling instability in tubes subject to internal and external axial fluid flow". *Proceedings of the 41st Conference on Dimensioning, 1971*.

[2] Païdoussis, M. P., Luu, T. P., and Prabhakar, S., 2008. "Dynamics of a long tubular cantilever conveying fluid downwards, which then flows upwards around the cantilever as a confined annular flow". *Journal of Fluids and Structures,* ***24***(1), pp. 111–128.

[3] Rinaldi, S., 2009. "Experiments on the dynamics of cantilevered pipes subjected to internal and/or external axial flow". Master's thesis, McGill University.

[4] Fujita, K., and Moriasa, A., 2015. "Stability of cantilevered pipes subjected to internal flow and external annular axial flow simultaneously". In ASME 2015 Pressure Vessels and Piping Conference, American Society of Mechanical Engineers, pp. V004T04A020–V004T04A020.

[5] Semler, C., Li, G. X., and Païdoussis, M. P., 1994. "The non-linear equations of motion of pipes conveying fluid". *Journal of Sound and Vibration,* ***169***(5), pp. 577–599.

[6] Lopes, J.-L., Païdoussis, M. P., and Semler, C., 2002. "Linear and nonlinear dynamics of cantilevered cylinders in axial flow. Part 2: The equations of motion". *Journal of Fluids and Structures,* ***16***(6), pp. 715–737.

[7] Lighthill, M. J., 1960. "Note on the swimming of slender fish". *Journal of Fluid Mechanics,* ***9***(2), pp. 305–317.

[8] Taylor, G. I., 1952. "Analysis of the swimming of long and narrow animals". *Proceedings of the Royal Society of London A: Mathematical, Physical and Engineering Sciences,* ***214***(1117), pp. 158–183.

[9] Doedel, E. J., Fairgrieve, T. F., Sandstede, B., Champneys, A. R., Kuznetsov, Y. A., and Wang, X., 2007. "Auto-07p: Continuation and bifurcation software for ordinary differential equations, 2007".